Ultrafast solvation dynamics at binding and active sites of photolyases

Chih-Wei Chang[a], Lijun Guo[a], Ya-Ting Kao[a], Jiang Li[a], Chuang Tan[a], Tanping Li[a], Chaitanya Saxena[a], Zheyun Liu[a], Lijuan Wang[a], Aziz Sancar[b], and Dongping Zhong[a,1]

[a]Departments of Physics, Chemistry, and Biochemistry, Programs of Biophysics, Chemical Physics, and Biochemistry, 191 West Woodruff Avenue, The Ohio State University, Columbus, OH 43210; [b]Department of Biochemistry and Biophysics, University of North Carolina School of Medicine, Chapel Hill, North Carolina 27599

Dynamic solvation at binding and active sites is critical to protein recognition and enzyme catalysis. We report here the complete characterization of ultrafast solvation dynamics at the recognition site of photoantenna molecule and at the active site of cofactor/substrate in enzyme photolyase by examining femtosecond-resolved fluorescence dynamics and the entire emission spectra. With direct use of intrinsic antenna and cofactor chromophores, we observed the local environment relaxation on the time scales from a few picoseconds to nearly a nanosecond. Unlike conventional solvation where the Stokes shift is apparent, we observed obvious spectral shape changes with the minor, small, and large spectral shifts in three function sites. These emission profile changes directly reflect the modulation of chromophore's excited states by locally constrained protein and trapped-water collective motions. Such heterogeneous dynamics continuously tune local configurations to optimize photolyase's function through resonance energy transfer from the antenna to the cofactor for energy efficiency and then electron transfer between the cofactor and the substrate for repair of damaged DNA. Such unusual solvation and synergetic dynamics should be general in function sites of proteins.

function-site solvation | ultrafast dynamics | spectral tuning | protein rigidity and flexibility | femtosecond-resolved emission spectra

Dynamic solvation in binding and active sites plays a critical role in protein recognition and enzyme reaction, and such local motions optimize spatial configurations and minimize energetic pathways (1–11). These dynamics involve local constrained protein and trapped-water motions within angstrom distance and occur on ultrafast time scales (6, 7, 10, 11). Typically, extrinsic dye molecules or synthetic amino acids were used as local optical probes to label function sites, and the local relaxations were observed, ranging from femtoseconds to nanoseconds (5, 12–14). Such labeling of bulky dye molecules usually induces significant local perturbations, and direct characterization with intrinsic chromophores in proteins eliminates those interferences and reveals intact environment responses (4, 7, 15–21), as recently examined in green fluorescence proteins (21). We have recently studied a series of flavoproteins using intrinsic flavin molecule as the optical probe (10, 22, 23) and especially found the important functional role of local solvation in photolyase (10).

Photolyase, a flavoprotein and a photoenzyme, repairs damaged DNA caused by UV irradiation. Two types of structurally similar photolyases are specific for two major UV-induced DNA lesions of cyclobutane pyrimidine dimer (CPD) and (6-4) photoproduct (24). The CPD photolyase contains two noncovalently bound chromophores, a pterin molecule in the form of methenyltetrahydrofolate (MTHF) in the binding site as the photoantenna for energy efficiency and a fully reduced flavin adenine dinucleotide (FADH⁻) at the active site as the catalytic cofactor for repair of damaged DNA. The (6-4) photolyase contains the same catalytic cofactor, but the antenna chromophore has not been well characterized. Fig. 1 shows the x-ray structures of both photolyases with chromophore molecules (25, 26). Both the x-ray

structures and molecular dynamics (MD) simulations (Fig. 1) show certain water molecules trapped at the binding and active sites, and charged and polar amino acids surrounding the chromophores of MTHF and FADH⁻. Thus, upon excitation the local polar environments of these function sites would proceed to a series of relaxations. Understanding of these local motions is crucial to their functional dynamics of resonance energy transfer from the photoantenna to the cofactor and electron transfer between the cofactor and the substrate in catalytic repair photocycle.

Our earlier studies on *Escherichia coli* CPD photolyase (EcPhr) showed that the active-site solvation is on the similar time scale of the catalytic reaction of electron transfer in hundreds of picoseconds, resulting in a nonequilibrium dynamic process and a direct modulation of charge separation (10, 27–29). The characterization of resonance energy transfer from the photoantenna (30, 31) revealed minor solvation at the binding site in less than 20 ps. To completely characterize the relaxation dynamics at the photoantenna MTHF binding pocket and the cofactor FADH⁻ active site, we isolate each chromophore in photolyase by eliminating the other chromophore through site-directed mutation and photodecomposition (32). Specifically, for the binding site of MTHF, we screened various mutants at the active sites of EcPhr and *Caulobacter crescentus* CPD photolyase (CcPhr) (33) to eliminate the binding of the cofactor FADH⁻. We finally obtained two mutants of EcPhr-N341A and CcPhr-W395R; the latter fully binds MTHF but not FADH⁻ at all, as shown by the absorption and emission spectra in Fig. 2. For the active site of FADH⁻, we removed the photoantenna molecule at the binding site through photodecomposition, and we studied both EcPhr and *Arabidopsis thaliana* (6-4) photolyase [At(6-4)] (Fig. 2). With femtosecond resolution, we mapped out the entire fluorescence dynamics and obtained the complete local relaxations of the binding and active sites in photolyases.

Results and Discussion

Ultrafast Fluorescence Transients and Function-Site Solvations. Figs. 3–5 show the femtosecond-resolved fluorescence transients for several typical wavelengths gated from the blue to red side of the chromophore's emissions of the CcPhr-W395R mutant, EcPhr-Wt, and At(6-4)-Wt, respectively. All transients were taken within a 3.2-ns time window. These transients exhibit ultrafast decay dynamics on picosecond time scales at the shorter wavelengths and gradually slow down toward the emission peaks, a manifestation of the local solvation dynamics. These fluorescence dynamics show a similar pattern of temporal behaviors with continuous solvation from a few to tens and to hundreds of picoseconds, but the solvation amplitudes at each time scale and for
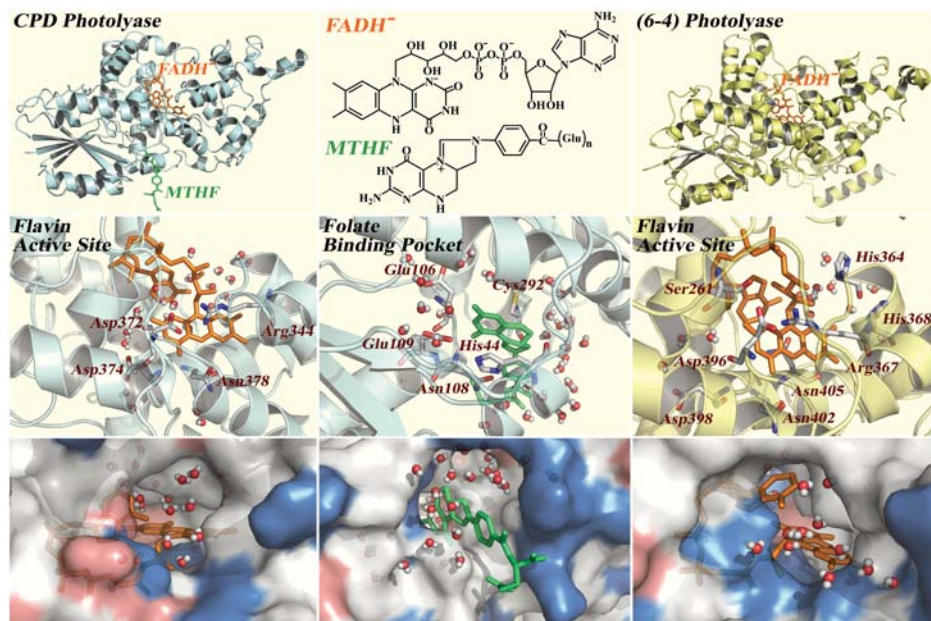
Fig. 1. *Top panel*: X-ray structures of *E. coli* CPD photolyase [*Left*, Protein Data Bank (PDB): 1DNP] and *A. thaliana* (6-4) photolyase (*Right*, PDB: 3FY4) with the photoantenna molecule (MTHF) and the cofactor (FADH⁻) in the center. *Middle panel*: Close-up view of the flavin active site (*Left*) and the folate binding pocket (*Middle*) of CPD photolyase and the active site of (6-4) photolyase (*Right*) with the neighboring polar/charged residues and trapped-water molecules within 8 Å from one snapshot of 1-ns MD simulations for each site. *Bottom panel*: Corresponding surface maps of the MD snapshots, showing the local topography, chemical property (red, negative charged residue; blue, positive charged residue), and trapped-water molecules at the three sites.

each site are very different. For the binding site of MTHF (Fig. 3), the solvation magnitude is smallest. Besides the long lifetime emission of 2.9 ns, we observed three decay components in approximately 3, 30–50, and 400–600 ps at the blue side from 420 to 460 nm. At 460–580 nm around the emission peak and at the red side, we observed two rise components in a few and tens of picoseconds; the latter is superimposed with the long decay components. However, at the far-red side, such as at 680 nm, we observed the fast and slow decay dynamics again (Fig. 3). Overall, the amplitudes of these solvation components are small and all less than 20% of the total signal. Because we excited MTHF at 400 nm around the absorption peak, we also examined the vibronic relaxation by tuning the pump wavelength to 320 nm and observed the cooling dynamics within 2 ps. Thus, the observed solvation dynamics mainly take place in tens and hundreds of picoseconds. Such slow relaxations with small amplitudes must reflect the local binding interactions as discussed below.

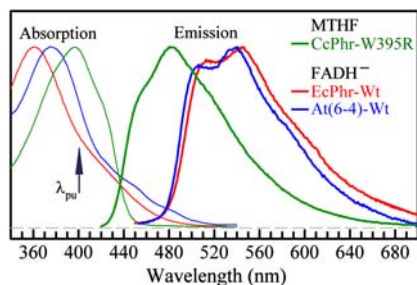For the active sites in the two photolyases (Figs. 4 and 5), the solvation dynamics are obvious. Besides the different long life-times of 1.3 ns for EcPhr-Wt and 3 ns for At(6-4)-Wt, both sites show large ultrafast decay components, and the relaxation in At (6-4) is even more significant. Similarly, at the blue side, we observed three decay components in 1–2.5, 21–35, and 400–550 ps for EcPhr and 0.9–2, 8–25, and 250–900 ps decay dynamics for At(6-4). The third long relaxation dynamics in EcPhr probably mixes with the lifetime decay (1.3 ns), resulting in a
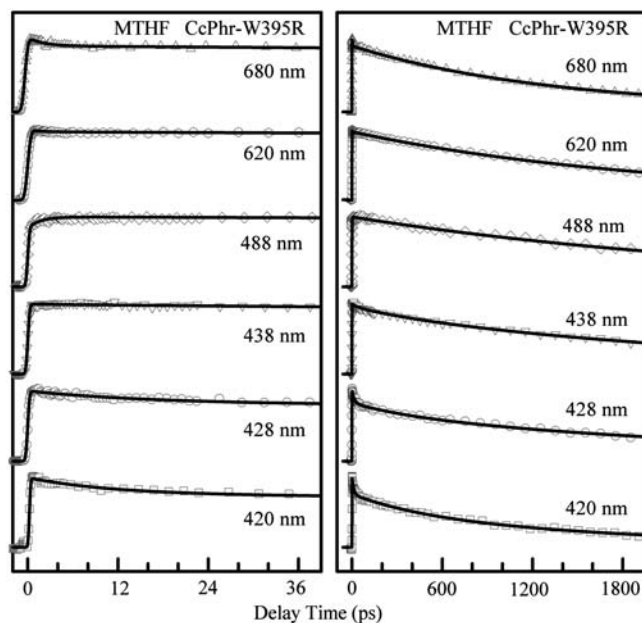

Fig. 2. Steady-state absorption (thin line) and emission (thick line) spectra of CcPhr-W395R (green), EcPhr-Wt (red), and At(6-4)-Wt (blue), respectively. The excitation wavelengths were 360 nm for EcPhr-Wt, 400 nm for At(6-4)-Wt, and 380 nm for CcPhr-W395R. For femtosecond experiments, $\lambda_{pu} = 400$ nm. For EcPhr-Wt and At(6-4)-Wt, the spectra were taken under anaerobic conditions, whereas for CcPhr-W395R the spectra were taken under aerobic conditions.

Fig. 3. Normalized femtosecond-resolved fluorescence transients of MTHF* in CcPhr-W395R for several gated emission wavelengths in short (*Left*) and long (*Right*) time ranges. The transients were gated from the far-blue (420 nm) to far-red side (680 nm). Note that around the peak at 480 nm, the transient shows an initial rise with long lifetime decay. At the far-red side, the transients exhibit fast decay dynamics again.
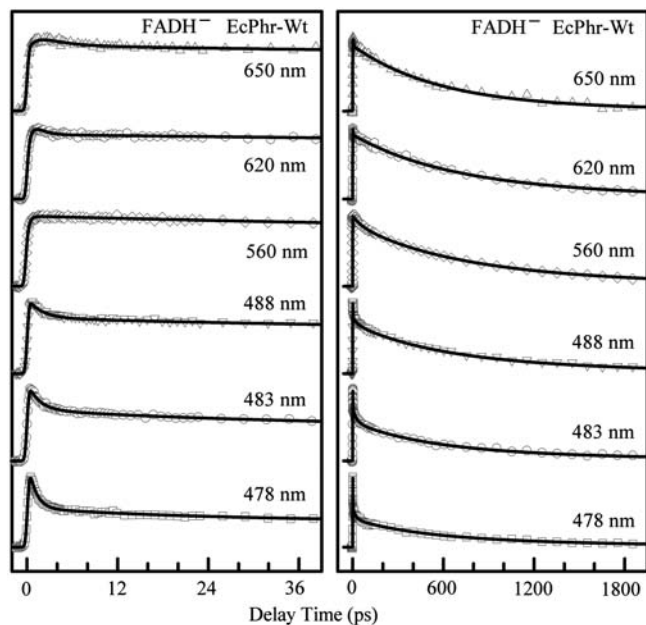
Fig. 4. Normalized femtosecond-resolved fluorescence transients of FADH^{-*} in EcPhr-Wt for several gated emission wavelengths in short (*Left*) and long (*Right*) time ranges. The transients were gated from the far-blue (478 nm) to far-red side (650 nm) and clearly show large ultrafast solvation components at the blue side. Note that near the peak, the transient at 560 nm shows long lifetime decay. At the far-red side, the transients exhibit fast decay dynamics again.

shorter time scale of 400–550 ps. All three components in At(6-4) have larger amplitudes, showing the significant solvation at the active site. At the far-red side, the transients display the fast and slow decay dynamics again as observed in MTHF*. Overall,
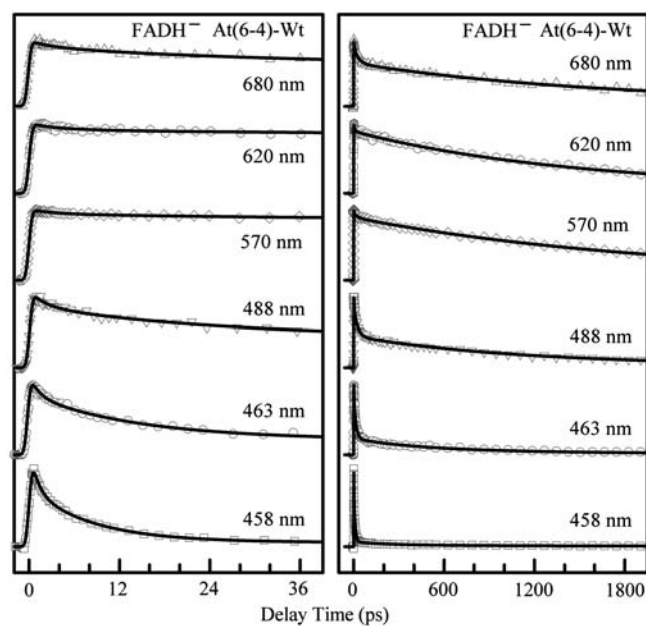

Fig. 5. Normalized femtosecond-resolved fluorescence transients of FADH^{-*} in At(6-4)-Wt for several gated emission wavelengths in short (*Left*) and long (*Right*) time ranges. The transients were gated from the far-blue (458 nm) to far-red side (680 nm) and show significant solvation dynamics. Note that near the peak, the transient at 570 nm shows long lifetime decay except a small fast decay component of 30 ps with 5–7% amplitude of the total signal, which is a fast deactivation process due to the flexible structure of FADH^{-*}. At the far-red side, the transients exhibit fast decay dynamics again.

both active sites are dynamic, and the distinct difference in the active-site solvation for the two photolyases reflects the different local structural and chemical properties.

Traditionally, we can construct femtosecond-resolved emission spectra using wavelength-resolved fluorescence transients obtained above to derive solvation correlation functions, for example, using the change of Stokes shifts with time (34). In doing so, we need to assume the emission spectra following a log-normal distribution. For MTHF*, the emission spectrum (Fig. 2) clearly shows certain features, similar to a vibronic structure often observed for dye molecules in nonpolar or rigid environments (35). For FADH^{-*}, the emission spectra (Fig. 2) show an irregular distribution with double peaks at 515 and 545 nm for EcPhr and 505 and 540 nm for At(6-4), which may be attributed to two possible ground-state isomers with the concave and convex structures of the isoalloxazine ring (36). Thus, given the heterogeneous electrostatic distributions and different structural flexibilities of the functional sites, to evaluate the complete local relaxation, we need to directly measure the femtosecond-resolved emission spectra and examine how the emission spectra change with local relaxation.

Femtosecond-Resolved Emission Spectra and Unusual Local Relaxations. Fig. 6 shows the three-dimensional representation of the emission spectrum evolution with time (*Top*) and a few snapshots at different delay times (*Bottom*) for the three sites. It is striking that the three spectral evolutions are dramatically different. Surprisingly, the emission spectra of MTHF* at the binding pocket exhibit a minor dynamic Stokes shift, at most tens of wavenumbers (cm^{-1}) in total. Overall, the solvation relaxation is very small. The emission spectrum at the delay time of 0.5 ps is similar to that at 2 ns except that the spectral width slightly narrows. Because both mutants of CcPhr-W395R and EcPhr-N341A show nearly the same absorption and emission spectra with the identical lifetime of 2.9 ns, the two binding pockets should have a similar environment. The x-ray structure shows at least 18 water molecules around the MTHF chromophore moiety of EcPhr within 8 Å. Among 18 water molecules, 15 water molecules are trapped inside the binding pocket, and the other three are near the pocket entrance. These water molecules must be very immobile, and their residence times are probably longer than nanoseconds. Surprisingly, our MD simulations in 1 ns even show more than 30 water molecules within 8 Å. Also, several polar/charged amino acid residues such as C292, H44, N108, E109, and E106 in EcPhr are in direct van der Waals contact with the chromophore moiety (Fig. 1). Clearly, the binding pocket is a highly polar environment. Recent theoretical calculations (37) reported a dipole-moment change of at least 1 debye (D) between the ground state and the first excited state of the pterin molecule. Thus, our observation of a minor Stokes shift must reflect a very rigid environment, consistent with the emission profile and transient dynamics. The observed relaxation dynamics in tens and hundreds of picoseconds thus represent the collective motions of trapped-water molecules and locally constrained polar/charged sidechains. These highly restricted, slow relaxations due to the local rigidity gradually tune the excited state, leading to the observed small peak and shape changes with time.

For FADH^{-*} at the active site of EcPhr-Wt, we observed only a small spectral shift but instead an obvious shape change at the blue side of the emission. The central distribution of the emission spectrum at 0.5 ps is already around the steady-state peaks. The x-ray structure shows four water molecules buried at the bottom of the active site and eight water molecules around the entrance of the active site within 8 Å from the isoalloxazine ring. Our MD simulations (1 ns) found 22 water molecules around the moiety ring (Fig. 1). There are at least four polar/charged sidechains of R344, N378, D372, and D374 in direct van der Waals contact with the moiety ring. Thus, the active site is also a highly polar
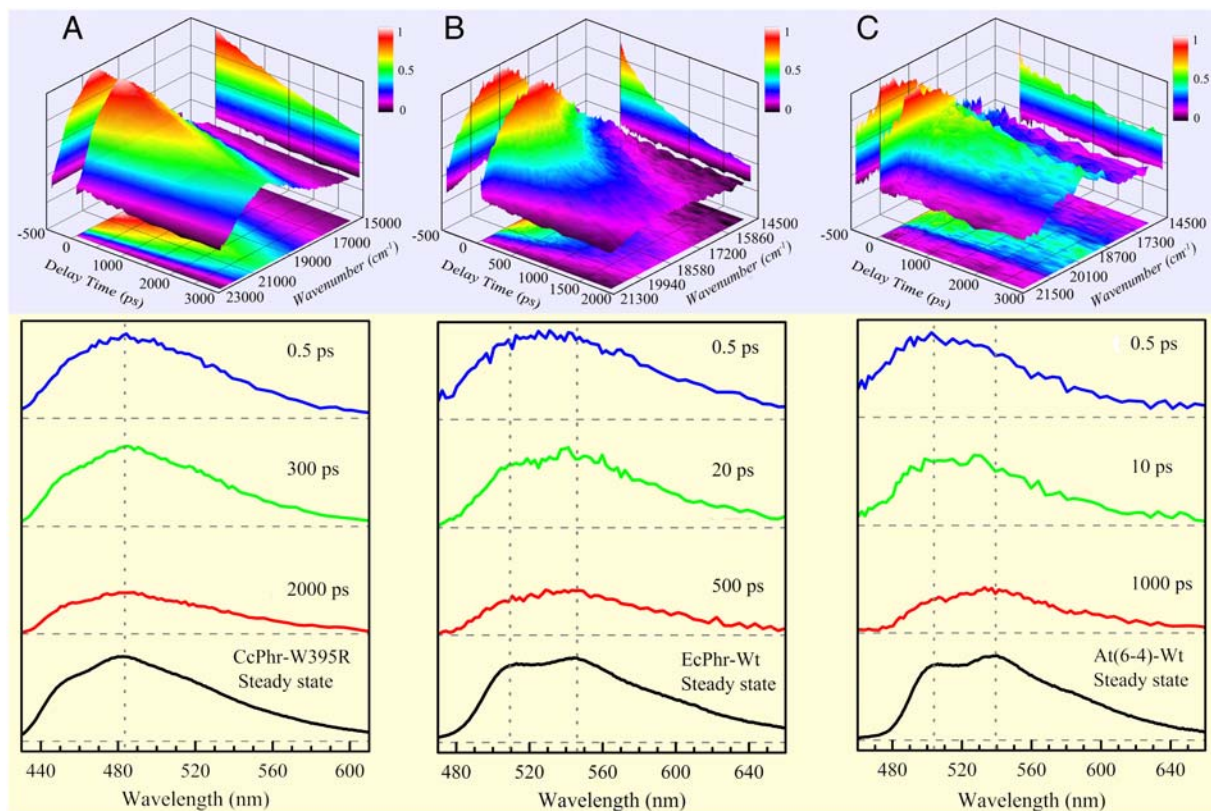
Fig. 6. *Upper panel*: 3D representation of femtosecond-resolved emission spectra of CcPhr-W395R (*A*), EcPhr-Wt (*B*), and At(6-4)-Wt (*C*) along time (ps) and emission energy (cm⁻¹). The intensity was scaled by a color code. *Lower panel*: Snapshots of femtosecond-resolved spectra at three typical delay times for the three sites with their corresponding steady-state emission spectra. For comparison and clarity, the steady-state emission peaks were marked by the gray dotted lines as references to show spectral peak and shape evolution.

environment. The dipole-moment change between the ground and excited states was recently reported to be more than 10 D (38), but we estimated that it should be around 1–2 D. Therefore, the observed small Stokes shift indicates a relatively rigid active site, but overall it is more flexible than the binding pocket of MTHF, especially the initial ultrafast relaxation as observed in the transients. The observed continuous solvation dynamics from a few to five hundreds of picoseconds again reflect the local collective motions of trapped-water molecules and polar/charged sidechains. These constrained motions induce only a small Stokes shift and stabilization energy, but strongly perturb the excited state, resulting in the obvious spectral shape changes.

The femtosecond-resolved emission spectra of FADH⁻* at the active site of At(6-4)-Wt are drastically different from those of EcPhr-Wt. We not only observed a significant spectral shape change but also a large spectral shift. At 0.5 ps, the spectrum peaks around 500 nm and at a later time of 1 ns, the peak moves to 540 nm. Clearly, the solvation relaxation is largest among the three sites. The x-ray structure shows only seven water molecules around the ring moiety within 8 Å with six buried inside the active site and one near the entrance. Our MD simulations (1 ns) show the least average water molecules of 14 near the ring moiety at the active site, consistent with the smaller hole size at the entrance shown in the x-ray structures for two photolyases (Fig. 1). However, there are more polar/charged amino acid residues such as H368, H364, N402, N405, S261, R367, D396, and D398 in direct van der Waals contact with the isoalloxazine ring (Fig. 1). Clearly, the active site is also a highly polar environment with dominant polar/charged sidechains. Thus, the significant relaxation reflects a relatively flexible active site with large plasticity, consistent with our transient observation. The observed large solvation in the transients results from the substantial motions of the

local trapped-water and flexible polar/charged sidechains, leading to a large Stokes shift. Meanwhile, such heterogeneous local motions greatly modulate the excited state, resulting in the significant spectral shape changes. The flexible active site is also supported by another observation. We observed a fast component of 30 ps with 5–7% amplitude in the transient gated at the emission peak (Fig. 5), a deactivation process through the butterfly and/or twist motions of the isoalloxazine ring as also shown in our recent studies of its homologous cryptochromes (22, 23). The different absorption spectra and distinct time-zero emission spectra in the two active sites (Figs. 2 and 6) also reflect the chromophore's different structural configurations and its heterogeneous structural and electrostatic environments. It would be erroneous if we conclude from the steady-state spectra that the FADH⁻* in EcPhr would have a larger dynamic Stokes shift, and in this case it has a smaller one.

Correlation Functions and Synergetic Dynamics. To extract the correlation functions for the three sites, the conventional method using the Stokes shift changes with time would not be applicable here. Alternatively, we can use the change of average frequencies with time. However, to avoid the possible cancellation in calculation of the average frequencies due to the narrowing of the spectral width, we also calculated the average frequencies only using the partial spectral profile at the blue side of the steady-state emission peak. Both results are shown in Fig. 7, using the stabilization-energy (relative to the time-zero average frequency) changes with time. The only main difference is the long component of the MTHF* solvation response, where the emission spectra do show narrowing at longer time. These correlation responses can be represented by

$$\Delta E = \Delta E_1 e^{-t/\tau_1} + \Delta E_2 e^{-t/\tau_2} + \Delta E_3 e^{-t/\tau_3} + \Delta E_\infty,$$
$$\Delta E_1 + \Delta E_2 + \Delta E_3 + \Delta E_\infty = 0. \qquad \textbf{[1]}$$

To further evaluate the local flexibility, we define an average solvation speed (or an average environment reorganization rate) to express how much energy drop (in cm^{-1}) per picosecond by local relaxation (20):

$$S_1 = \frac{\Delta E_1}{\tau_1}, \qquad S_2 = \frac{\Delta E_2}{\tau_2}, \qquad S_3 = \frac{\Delta E_3}{\tau_3}. \qquad \textbf{[2]}$$

All derived results for the three sites are given in Table 1. These results clearly show different solvation magnitudes and speeds for the three sites. Overall, the binding site has the smallest shift of only 39 cm^{-1}, and its three solvation speeds are slowest, well below those of the other two sites, reflecting the rigid binding interactions between the photoantenna molecule and the protein. This strong recognition implies a rigid orientation of MTHF* and a largest spectral overlap with the cofactor's absorption for efficient energy transfer.

For the two active sites, the spectral shift of At(6-4)-Wt is about three times larger than that of EcPhr-Wt, reaching to 798 cm^{-1}. It is striking that both sites have the similar first (S_1) and third (S_3) solvation speeds but with a significant difference in the second one (S_2). Both sites have all similar three relaxation time scales, comparable first and third stabilization energies, but very different second stabilization energies. The first ultrafast relaxation in a few picoseconds mostly results from the local reorientation motions of trapped water molecules and/or neighboring unscreened polar/charged sidechains. Thus, the comparable time scale, stabilization energy, and solvation speed indicate that both sites have the similar polar environment and initial ultrafast response. The second relaxation in tens of picoseconds reflects the coupled water-protein motions, a collective rearrangement of the local configuration (19, 20, 39). Although both sites have a similar time scale of approximately 20 ps, the At(6-4)-Wt has a stabilization energy of 471 cm^{-1}, about ten times larger than that of EcPhr-Wt, leading to a significantly larger solvation speed. This observation shows again the more flexible active site of At(6-4). Because the active site of At(6-4) has more polar/charged sidechains, the second relaxation mostly comes from those sidechains in direct contact with the chromophore. This result is significant and reflects larger mobility of protein sidechains in the At(6-4) active site. On the other hand, the protein sidechains at the active site of EcPhr are much less mobile. These distinct local dynamics in the two active sites correlate well with their functions. For EcPhr, to maximize energy transfer from the antenna molecule (MTHF) and optimize the catalytic reactions of electron transfer with the CPD substrate and the CPD splitting, a rigid active site with local flexible orientation motions would be ideal (40). For At(6-4), to optimize both electron and proton transfers, especially the sensitive proton transfer from the neighboring sidechain (26, 41), the extra flexibility of sidechains would be necessary to search for the favorable configuration for proton tunneling. Finally, the third relaxation with the similar time scale in subnanosecond, stabilization energy in tens of wavenumbers, and solvation speed represents the intrinsic collective active-site protein motions, the same for both photolyases.

Conclusion

We reported our complete characterization of the local solvation dynamics at the binding pocket of the photoantenna molecule and at the two active sites of the cofactor/substrate in three photolyases. These relaxation processes at the function sites are critical to understanding functional dynamics of efficient energy transfer and catalytic reactions for repair of damaged DNA by photolyases. With site-directed mutagenesis and photodecomposition, we isolated each chromophore at the functional site. Without extrinsic labeling, we used the antenna molecule and cofactor as the local optical probes and systematically examined the fluorescence dynamics with femtosecond resolution. With femtosecond-resolved emission spectra, for all three function sites we observed all apparent spectral shape changes with the minor, small, and large spectral shifts for the antenna binding site, CPD photolyase active site, and (6-4) photolyase active site, respectively. These striking solvation dynamics, resulting from differently constrained polar/charged-sidechain and trapped-water motions, occur on wide time scales from a few picoseconds to nearly a nanosecond and continuously modulate the chromophore's excited states to optimize the function dynamics for biological efficiency. These series of relaxations correlate well with the rigidity and flexibility of the function sites, and we observed a very rigid antenna binding site, a relatively rigid active site in CPD photolyase but with large local orientation flexibility, and a flexible active site in (6-4) photolyase with both considerable local orientation flexibility and sidechain mobility. Such unconventional solvation dynamics even shown at far-red–side emission (42) with rich spectral evolution in heterogeneous structural and chemical environments should be general for functional sites of proteins, as recently shown in green fluorescent proteins (43).

Materials and Methods

Protein Preparation. The purifications of EcPhr-Wt, CcPhr-W395R, and At(6-4)-Wt photolyases have been described in detail elsewhere (33, 44, 45). In all the femtosecond-resolved experiments, we used the concentrations of 300 μM for EcPhr-Wt and At(6-4)-Wt and 100 μM for CcPhr-W395R mutant in 50% (vol/vol) glycerol with a buffer of 50 mM Tris-HCl (pH 7.4), 100 mM NaCl, 1 mM EDTA, and 5 mM dithiothreitol. Both EcPhr-Wt and At(6-4)-Wt were purified with neutral radical FADH⁻ and/or oxidized FAD forms and then
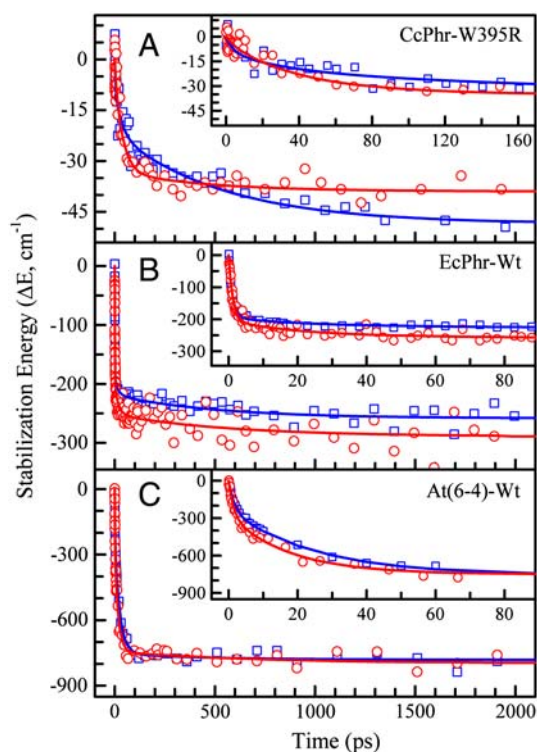

Fig. 7. Solvation correlation functions using the stabilization-energy changes with time for the binding site of CcPhr-W395R (*A*) and the actives sites of EcPhr-Wt (*B*) and At(6-4)-Wt (*C*). The stabilization energy was calculated using the average frequency relative to its time-zero one. Two relaxation responses were shown for each site by employing two methods for calculation of the average frequency using either the entire emission spectrum (red) or only the blue-side portion before the emission peak (blue).

Table 1. Results of the solvation dynamics in binding and active sites in three photolyases*

Chromophore	Protein	τ_1	ΔE_1	τ_2	ΔE_2	τ_3	ΔE_3	S_1	S_2	S_3	ΔE
MTHF	CcPhr-W395R†	4	3	38	30	450	6	0.75	0.79	0.01	39
FADH⁻	EcPhr-Wt	1.2	204	20	48	580	37	170	2.4	0.06	289
	At(6-4)-Wt	1.4	274	17	471	730	53	196	27.7	0.07	798

*The time constant (τ), stabilization energy (ΔE), and solvation speed (S) are in units of ps, cm⁻¹, and cm⁻¹/ps, respectively.
†The results are different from those solvation dynamics derived by using only the blue-side spectrum before 480 nm to calculate the average frequencies, where the time constants are similar, $\tau_1 = 4$ ps, $\tau_2 = 35$ ps, and $\tau_3 = 540$ ps, but the stabilization energies are different, $\Delta E_1 = 9$ cm⁻¹, $\Delta E_2 = 13$ cm⁻¹, and $\Delta E_3 = 27$ cm⁻¹.

converted to a fully reduced FADH⁻ form under anaerobic conditions. The absorption and emission spectra were taken to confirm only the single chromophore in each photolyase (Fig. 2).

Femtosecond Methods. All the femtosecond-resolved measurements were carried out using the fluorescence up-conversion method. The experimental method has been detailed elsewhere (42). Briefly, the pump wavelength was set at 400 nm, and its pulse energy typically was attenuated to 140–200 nJ. The instrument response time under the current noncollinear geometry is about 450 fs, and all data were taken at a magic angle (54.7°). The time-resolved emission spectra at various delay times were obtained by scanning the mixing crystal angles and monochromator wavelengths simultaneously over the entire emission range. A variety of delay times were appropriately chosen to reconstruct the 3D spectra (Fig. 6). The time zero at each wavelength was carefully calibrated. We calculated the average frequency $\nu(t)$ (46) and then evaluated the stabilization energy (relative to the time-zero average frequency) to deduce the solvation correlation responses (Fig. 7).

1. Levy Y, Onuchic JN (2006) Water mediation in protein folding and molecular recognition. *Annu Rev Biophys Biomol Struct* 35:389–415.
2. Pal SK, Zewail AH (2004) Dynamics of water in biological recognition. *Chem Rev* 104:2099–2123.
3. Mattos C (2002) Protein-water interactions in a dynamic world. *Trends Biochem Sci* 27:203–208.
4. Zhong D (2009) Hydration dynamics and coupled water-protein fluctuations probed by intrinsic tryptophan. *Adv Chem Phys* 143:83–49.
5. Zhong D, Pal SK, Zewail AH (2001) Femtosecond studies of protein-DNA binding and dynamics: Histone I. *ChemPhysChem* 2:219–227.
6. Zhong D, Douhal A, Zewail AH (2000) Femtosecond studies of protein-ligand hydrophobic binding and dynamics: Human serum albumin. *Proc Natl Acad Sci USA* 97:14056–14061.
7. Qiu W, et al. (2006) Ultrafast solvation dynamics of human serum albumin: Correlations with conformational transitions and site-selected recognition. *J Phys Chem B* 110:10540–10549.
8. Helms V (2007) Protein dynamics tightly connected to the dynamics of surrounding and internal water molecules. *ChemPhysChem* 8:23–33.
9. Pocker Y (2000) Water in enzyme reactions: Biophysical aspects of hydration-dehydration processes. *Cell Mol Life Sci* 57:1008–1017.
10. Kao Y-T, Saxena C, Wang L, Sancar A, Zhong D (2005) Direct observation of thymine dimer repair in DNA by photolyase. *Proc Natl Acad Sci USA* 102:16128–16132.
11. Qiu W, et al. (2007) Dissection of complex protein dynamics in human thioredoxin. *Proc Natl Acad Sci USA* 104:5366–5371.
12. Pierce DW, Boxer SG (1992) Dielectric-relaxation in a protein matirx. *J Phys Chem* 96:5560–5566.
13. Cohen BE, et al. (2002) Probing protein electrostatics with a synthetic fluorescent amino acid. *Science* 296:1700–1703.
14. Jesenská A, et al. (2009) Nanosecond time-dependent stokes shift at the tunnel mouth of haloalkane dehalogenases. *J Am Chem Soc* 131:494–501.
15. Homoelle BJ, Edington MD, Diffey WM, Beck WF (1998) Stimulated photon-echo and transient-grating studies of protein-matrix solvation dynamics and interexciton-state radiationless decay in α phycocyanin and allophycocyanin. *J Phys Chem B* 102:3044–3052.
16. Pal SK, Peon J, Zewail AH (2002) Biological water at the protein surface: Dynamical solvation probed directly with femtosecond resolution. *Proc Natl Acad Sci USA* 99:1763–1768.
17. Qiu W, et al. (2005) Ultrafast hydration dynamics in melittin folding and aggregation: Helix formation and tetramer self-assembly. *J Phys Chem B* 109:16901–16910.
18. Qiu W, et al. (2006) Protein surface hydration mapped by site-specific mutations. *Proc Natl Acad Sci USA* 103:13979–13984.
19. Zhang L, et al. (2007) Mapping hydration dynamics around a protein surface. *Proc Natl Acad Sci USA* 104:18461–18466.
20. Zhang L, Yang Y, Kao Y-T, Wang L, Zhong D (2009) Protein hydration dynamics and molecular mechanism of coupled water-protein fluctuations. *J Am Chem Soc* 131:10677–10691.
21. Abbyad P, Childs W, Shi X, Boxer SG (2007) Dynamic Stokes shift in green fluorescent protein variants. *Proc Natl Acad Sci USA* 104:20189–20194.
22. Kao Y-T, et al. (2008) Ultrafast dynamics and anionic active states of the flavin cofactor in cryptochrome and photolyase. *J Am Chem Soc* 130:7695–7701.
23. Kao Y-T, et al. (2008) Ultrafast dynamics of flavins in five redox states. *J Am Chem Soc* 130:13132–13139.
24. Sancar A (2003) Structure and function of DNA photolyase and cryptochrome blue-light photoreceptors. *Chem Rev* 103:2203–2237.
25. Park HW, Kim ST, Sancar A, Deisenhofer J (1995) Crystal structure of DNA photolyase from *Escherichia coli*. *Science* 268:1866–1872.
26. Maul MJ, et al. (2008) Crystal structure and mechanism of a DNA (6-4) photolyase. *Angew Chem Int Ed* 47:10076–10080.
27. Zhong D (2007) Ultrafast catalytic processes in enzymes. *Curr Opin Chem Biol* 11:174–181.
28. Kao Y-T, Saxena C, Wang L, Sancar A, Zhong D (2007) Femtochemistry in enzyme catalysis: DNA photolyase. *Cell Biochem Biophys* 48:32–44.
29. Wang H, Saxena C, Quan D, Sancar A, Zhong D (2005) Femtosecond dynamics of flavin cofactor in DNA photolyase: Radical reduction, local solvation, and charge recombination. *J Phys Chem B* 109:1329–1333.
30. Saxena C, Sancar A, Zhong D (2004) Femtosecond dynamics of DNA photolyase: Energy transfer of antenna initiation and electron transfer of cofactor reduction. *J Phys Chem B* 108:18026–18033.
31. Zheng X, Garcia J, Stuchebrukhov AA (2008) Theoretical study of excitation energy transfer in DNA photolyase. *J Phys Chem B* 112:8724–8729.
32. Heelis PF, Payne G, Sancar A (1987) Photochemical properties of *Escherichia coli* DNA photolyase: Selective photodecomposition of the second chromophore. *Biochemistry* 26:4634–4640.
33. Öztürk N, et al. (2008) Purification and characterization of a type III photolyase from *Caulobacter crescentus*. *Biochemistry* 47:10255–10261.
34. Lu W, Kim J, Qiu W, Zhong D (2004) Femtosecond studies of tryptophan solvation: Correlation function and water dynamics at lipid surfaces. *Chem Phys Lett* 388:120–126.
35. Oskouei AA, et al. (2008) Ultrafast UV photon echo peak shift and fluorescence up conversion studies of non-polar solvation dynamics. *Chem Phys* 350:104–110.
36. Nakai S, Yoneda F, Yamabe T (1999) Theoretical study on the lowest-frequency mode of the flavin ring. *Theor Chem Acc* 103:109–116.
37. Chen X, Xu X, Cao Z (2007) Theoretical study on the singlet excited state of pterin and its deactivation pathway. *J Phys Chem A* 111:9255–9262.
38. Prytkova TR, Beratan DN, Skourtis SS (2007) Photoselected electron transfer pathways in DNA photolyase. *Proc Natl Acad Sci USA* 104:802–807.
39. Li T, Hassanali AA, Kao Y-T, Zhong D, Singer SJ (2007) Hydration dynamics and time scales of coupled water-protein fluctuations. *J Am Chem Soc* 129:3376–3382.
40. Antony J, Medvedev DM, Stuchebrukhov AA (2000) Theoretical study of electron transfer between the photolyase catalytic cofactor FADH⁻ and DNA thymine dimer. *J Am Chem Soc* 122:1057–1065.
41. Hitomi K, et al. (2001) Role of two histidines in the (6-4) photolyase reaction. *J Biol Chem* 276:10103–10109.
42. Zhang L, Kao Y-T, Qiu W, Wang L, Zhong D (2006) Femtosecond studies of tryptophan fluorescence dynamics in proteins: Local solvation and electronic quenching. *J Phys Chem B* 110:18097–18103.
43. Shi X, et al. (2007) Ultrafast excited-state dynamics in the green fluorescent protein variant S65T/H148D. 2. Unusual photophysical properties. *Biochemistry* 46:12014–12025.
44. Sancar A, Smith FW, Sancar GB (1984) Purification of *Escherichia coli* DNA photolyase. *J Biol Chem* 259:6028–6032.
45. Li J, Uchida T, Todo T, Kitagawa T (2006) Similarities and differences between cyclobutane pyrimidine dimer photolyase and (6-4) photolyase as revealed by resonance Raman spectroscopy: Electron transfer from the FAD cofactor to ultraviolet-damaged DNA. *J Biol Chem* 281:25551–25559.
46. Maroncelli M, Fleming GR (1987) Picosecond solvation dynamics of coumarin 153: The importance of molecular aspect of solvation. *J Chem Phys* 86:6221–6239.

BIOPHYSICS AND COMPUTATIONAL BIOLOGY

CHEMISTRY